RSC Advances

PAPER

View Article Online
View Journal | View Issue

Cite this: *RSC Adv.*, 2024, **14**, 14793

Structural insights into novel therapeutic deep eutectic systems with capric acid using 1D, 2D NMR and DSC techniques with superior gut permeability†

Bayan Alkhawaja,[a] Faisal Al-Akayleh,*[a] Jehad Nasereddin,[b] Muhammad Kamran,[c] Tim Woodman,[d] Zaid Al-Rubaye,[a] Nidal Qinna,[a] Mayyas Al-Remawi[a] and Ali R. Olaimat[e]

Therapeutic deep eutectic solvents (THEDSs) are the best exemplification of green alternative formulations of active pharmaceutical ingredients (APIs) that offer superlative properties of APIs. Previously, THEDESs of risperidone, fentanyl and levofloxacin with capric acid (CA) were developed by our group. These APIs share cyclic tertiary amine nuclei. Herein, DESs of two drugs bearing cyclic tertiary amine nucleus, namely, droperidol and aripiprazole, in the presence of CA, were investigated as model drugs. Comprehensive analyses were conducted using liquid-state 1D and 2D NMR and differential scanning calorimetry (DSC) to elucidate the regiochemistry and thermodynamic mechanisms bringing about those THEDESs. Everted gut sac technique was used to study the flux of the developed THEDESs. 1D and 2D NMR techniques analyses revealed the importance of cyclic tertiary amine nuclei in forming interactions with CA. This was confirmed by the downfield shift of the protons proximal to the tertiary amine groups compared to the individual drugs. Diffusion NMR analysis (DOSY) showed a significant reduction in the diffusion coefficient of CA in the mixed system compared with CA in isolation. Thermal analysis of the two drugs revealed that the drugs have a low tendency to recrystallise upon melting but rather vitrify from a melt to form an amorphous solid. Interestingly, the superior absorption and flux of the THEDES formulation of droperidol was demonstrated using the ERIS. Collectively, this work provides a green method to attain liquid formulations of APIs with enhanced pharmacokinetic features.

Received 26th February 2024
Accepted 29th April 2024

DOI: 10.1039/d4ra01469c

rsc.li/rsc-advances

1 Introduction

Deep eutectic solvents (DESs) are mixtures of hydrogen bond donors (HBDs) and hydrogen bond acceptors (HBAs) with considerably lower melting points than their individual components. DESs are generally prepared by direct mixing or mechanical grinding in solvent-free conditions, sometimes with heating of the components in specific molar ratios.[1–3] DESs are a highly versatile group of low-melting systems brought about due to the increase of the system entropy.[4] DESs possess attractive features, encompassing thermal and chemical stability, low vapour pressure, high viscosity, and low flammability. In addition, due to their attractive versatility, DESs could be tailored and prepared according to the deviated aims, rendering them task-specific solvents, hence offering ubiquitous applications.[5,6] Globally, interest in finding safer and easier-to-handle alternatives to organic solvents has gained significant attention. Consequently, DESs could provide greener and less toxic substitutes for organic counterparts.[7–10]

Owing to their versatility, biocompatibility, and sustainability, DESs are increasingly involved in a multitude of pharmaceutical applications.[11,12] Ranging from being solvents for active pharmaceutical ingredients (APIs) to being utilised in drug delivery systems, DESs offered widespread advantages in the pharmaceutical realm. To this end, many recent reports displayed the utility of DESs in enhancing drug solubility of poorly soluble drugs,[10,13–15] permeability,[9] stability,[16] drug delivery, as well as being involved in the synthesis and extraction of active pharmaceutical ingredients.[17]

More interestingly, DESs of APIs, where the API acts as a component of the DES or IL, or what is known as therapeutic DESs (THEDESs), is another direct application of enhancing the

[a]*Faculty of Pharmacy and Medical Sciences, University of Petra, Amman, Jordan. E-mail: falakayleh@uop.edu.jo*

[b]*Department of Pharmaceutical Sciences, Faculty of Pharmacy, Zarqa University, Zarqa, 13110, Jordan*

[c]*Department of Chemistry, University of Bath, Claverton Down, BA2 7AY, Bath, UK*

[d]*Department of Life Sciences, University of Bath, Claverton Down, BA2 7AY, Bath, UK*

[e]*Drug Directorate, Jordan Food and Drug Administration, Shafa Badran, Amman, 11181, Jordan*

† Electronic supplementary information (ESI) available. See DOI: https://doi.org/10.1039/d4ra01469c

Table 1 Chemical structure and characteristics of the APIs that formed DESs with CA along with CA and MC structures

API	Structure	pK_a	Solubility[a]	T_m (°C)	Medical uses	Ref.
Risperidone	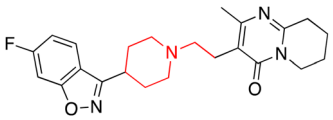	8.76	2.16	171 (ref. 28)	Treatment of schizophrenia, bipolar mania and psychosis	29
Fentanyl	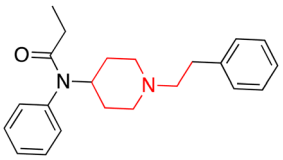	8.99 (ref. 30)	0.2	83–84	Opioid analgesic for pain management	30 and 31
Levofloxacin	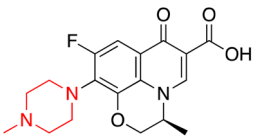	Basic pK_a 8.12 and acidic pK_a 6.1	Sparingly soluble	225–227	Broad-spectrum antibacterial drug	25, 32 and 33
Droperidol (Drp)	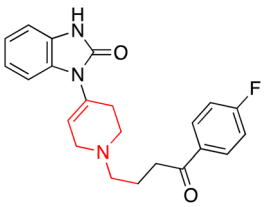	7.46	4.21	145–146.5	Management of the nausea and vomiting in surgical and diagnostic procedures	34 and 35
Aripiprazole (Arp)	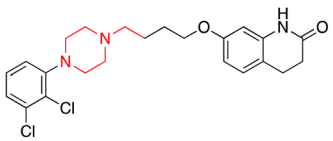	7.6	0.045	137–140	Treatment of many forms of mood and psychotic disorders	36
Capric acid (CA)	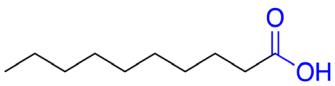	4.9	0.062	31.5	—	37
Methyl caprate (MC)	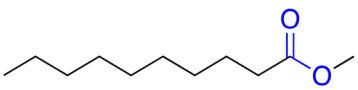	—	0.004[b]	−18.0	—	38

[a] Aqueous solubility at 25 °C, all records were obtained from PubChem.[27] [b] Solubility at 20 °C. T_m (melting point).

pharmaceutical characteristics in a safer and greener approach.[18] Forming the so-called hydrophobic DES, fatty acid-based DESs have been applied in various potential non-aqueous administrations.[18–21] Previously, DESs based on fatty acids have been formed with a multitude of APIs, such as menthol,[22] fentanyl,[23] propranolol,[24] risperidone[18] and levofloxacin.[25] The most significant advantage of DES based on biocompatible fatty acids is the realisation of these properties under mild and solventless conditions.[26]

The common consensus within the literature is that hydrogen bond interactions are the main interactions bringing about the formation of DES.[22] In-depth evaluation of the literature in the field of DESs and THEDESs has highlighted the limited understanding of the structural aspects of such systems, including predicting the propensity to form hydrogen bond interactions based on the chemical structure of APIs, thermodynamic behaviour or physical characteristics related to the lattice properties of the crystals of DES formers.

In our endeavours to generate deep understanding of DESs, we present in this work two novel THEDESs. Studying their chemical structures, some THEDEs with CA, such as fentanyl, risperidone and levofloxacin, share a cyclic tertiary amine moiety (Table 1).[18,25] Therefore, we envisaged evaluating the interactions between APIs possessing similar nuclei and CA, primarily using 1D and 2D NMR and DSC techniques. The selection criteria of the drugs in this work, namely droperidol (Drp) and aripiprazole (Arp), was based on their chemical structure; hence, we anticipated similar interactions. Building upon our previous findings, the primary aim of this work is to underline the regiochemistry and thermodynamic interactions taking place in two novel THEDESs with CA. Furthermore, we sought to study the direct application of this system through the evaluation of the absorption and permeation of the THEDSs of Drp using the everted rat intestinal sac (ERIS) technique.

2 Results and discussion

2.1 1D and 2D NMR studies

2.1.1 Eutectic mixtures of CA and Drp. Drp is a neuroleptic pharmaceutical agent that is commonly administered as an intravenous or intramuscular injection for the management of nausea and vomiting, acute psychosis and acute behavioural disturbance, as well as the management of migraine and vertigo.[39–41] It is practically insoluble in water and only sparingly soluble in alcohol (Table 1). Recent studies were focused on enhancing the solubility of Drp.[42] Hence, establishing a well-

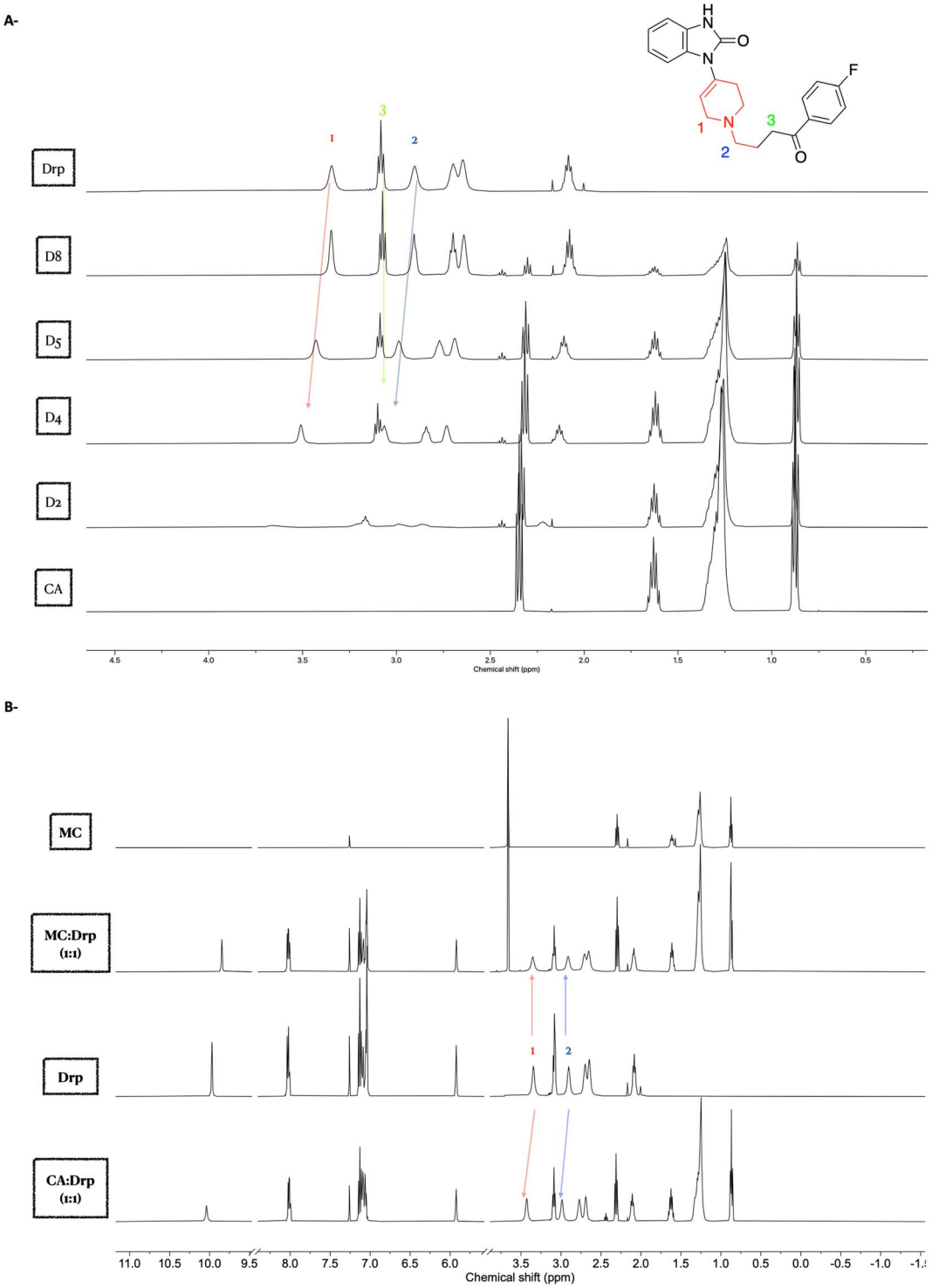

Fig. 1 ^{1}H NMR spectra of Drp–CA eutectic mixtures. (A) ^{1}H NMR spectra of Drp and CA eutectic mixtures in $CDCl_3$ solvent with expansion around the upper field region of the NMR spectrum, revealing the downfield shifting protons at 3.35 and 2.90 ppm with the increasing of CA molar ratio. (B) ^{1}H NMR spectra of Drp–CA and Drp–MC equimolar mixtures in $CDCl_3$ solvent.

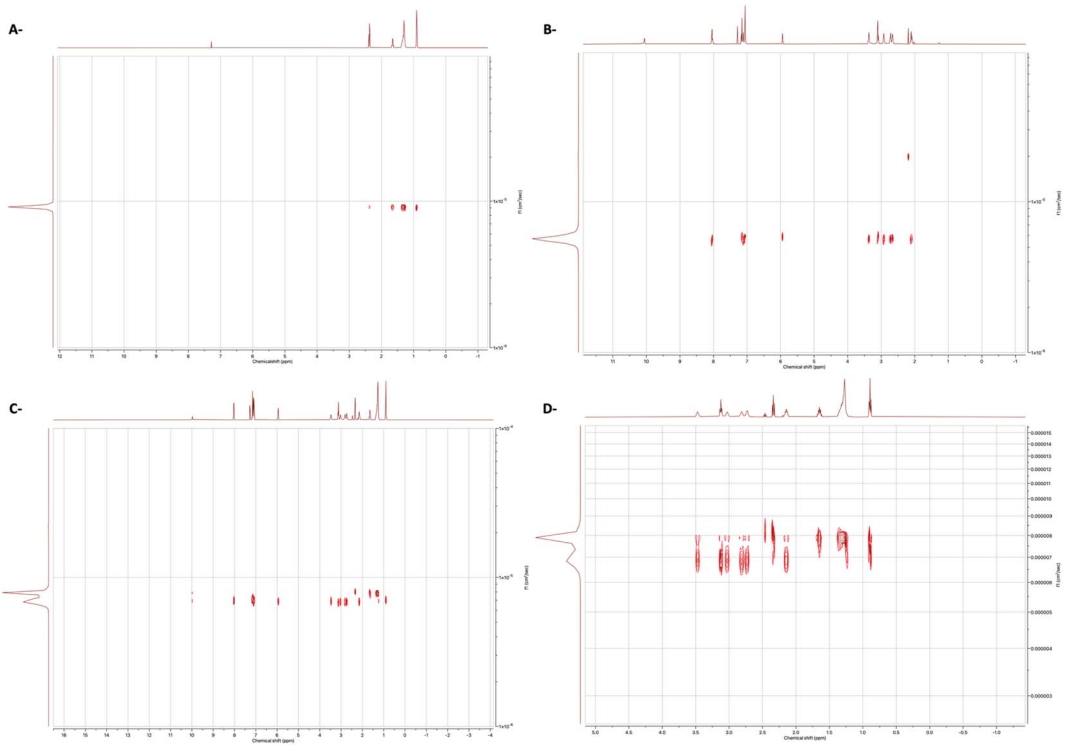

Fig. 2 DOSY ^{1}H spectra of (A) CA, (B) Drp, (C) binary 1 : 1 mixture of Drp and CA and (D) binary 1 : 1 mixture of Drp and CA with expansion. The solvent was $CDCl_3$.

defined DES between Drp and CA could be advantageous in improving its bioavailability and pharmacokinetic properties.

The plausible interaction behind the formed DES is the hydrogen bond interaction between CA and Drp, as seen previously with DES between CA and menthol.[43] To investigate this further, Drp and CA binary mixtures were prepared by increasing the molar ratio of Drp to CA by physical mixing. Amongst the prepared mixtures, D1 (0.9 : 0.1), D2 (0.8 : 0.2) and D3 (0.7 : 0.3) transformed into liquid form, whereas the rest of the binary mixtures transformed into a pasty form (Table 3). Initially, the binary mixtures were investigated by 1D and 2D NMR experiments.

It is well established that hydrogen bonding interactions could cause a downfield shift (higher frequency) of the carboxylic acid protons due to the deshielding effect.[44] However, our system couldn't assign the carboxylic acid protons due to their exchangeability (Fig. S1†). Hence, we focused on the change of the chemical shifts of Drp protons. To this end, comparing the chemical shifts between the different mixtures of CA and Drp, most of the protons of Drp exhibited no change in their chemical shifts with the increasing ratio of CA (Fig. S1†).

Nevertheless, a significant downfield shift was observed for the protons located at 3.35 ppm (1) and 2.90 ppm (2), assigned to the protons adjacent to the piperidine ring (Fig. 1A). The positive $\Delta\delta$ (chemical shift deviation) was calculated for the protons at 3.35 ppm (1) and 2.90 ppm (2) of Drp with CA and found to be 0.08 ppm and 0.09 ppm, respectively. These shifts indicate that these protons are either deshielded or the electron density is altered due to the interactions between the piperidine amine and the carboxylic acid of the CA. The observed downfield shift was also reported previously, where the proximal protons of the cyclic tertiary amine of levofloxacin.[25]

The tertiary amine group of the piperidine ring is expected to interact with CA by forming a hydrogen bond. Therefore, the proximal protons to the piperidine amine are anticipated to be in a new chemical environment due to this newly formed interaction. It is known that the formation of hydrogen bonding with the amine group leads to the increase in the acidity of the proximal protons, and hence, this could explain the observed downfield shift of the protons (1) and (2) (Fig. 1A).[45] Their chemical shifts reflect the chemical environment of the protons, the more the electron-withdrawing effect surrounding the protons (more acidic protons), the higher the resonance frequency (higher chemical shift) will be observed. The presence of the neighbouring hydrogen has caused the downfield shift of the proximal protons, as outlined above. In contrast, distal protons to the piperidine ring, such as proton at 3.08 ppm (3), did not exhibit such change in the chemical shift (Fig. 1A).

Table 2 Diffusion coefficients, F ($cm^2\ s^{-1}$) for individual molecules in chloroform and their 1 : 1 complexes

Compound	F_{CA} ($\times10^{-6}$)	F_{Drp} ($\times10^{-6}$)	F_{MC} ($\times10^{-5}$)	F_{Drp} ($\times10^{-6}$)
Individual component	9.03	5.72	1.15	5.72
Binary mixture (1 : 1)	7.82	6.79	1.06	5.33

To validate the observed ^{1}H NMR shifts in the eutectic mixtures and to draw more comprehensive conclusions around the underlying interactions between Drp and CA, we set out to compare the interaction between the eutectic mixture of both CA and Drp with the binary mixture of methyl ester caprate (MC) and Drp. MC lacks the CA hydroxy group and hence is incapable of being a hydrogen bond donor with Drp. To this end, MC and Drp binary mixtures were prepared at equimolar ratio, and their ^{1}H NMR spectra were compared. The positive $\Delta\delta$ (chemical shift deviation) of the protons at 3.35 ppm (1) and 2.90 ppm (2) of Drp with CA (0.08 ppm and 0.09 ppm, respectively) as observed earlier were not observed in the case of a binary mixture of Drp and MC (Fig. 1B). The attained results confirm the essential role of the carboxylic acid group of CA in forming the eutectic mixture with Drp.

Next, we set out to study the interactions using ^{1}H Diffusion NMR spectroscopy experiments of the binary mixtures and individual components in the $CDCl_3$. Diffusion NMR experiments, sometimes called DOSY (Diffusion Ordered Spectroscopy), provide a means for studying the interactions between the compounds by providing a 2D spectrum in which one axis is the chemical shift while the other is the diffusion coefficient.[46]

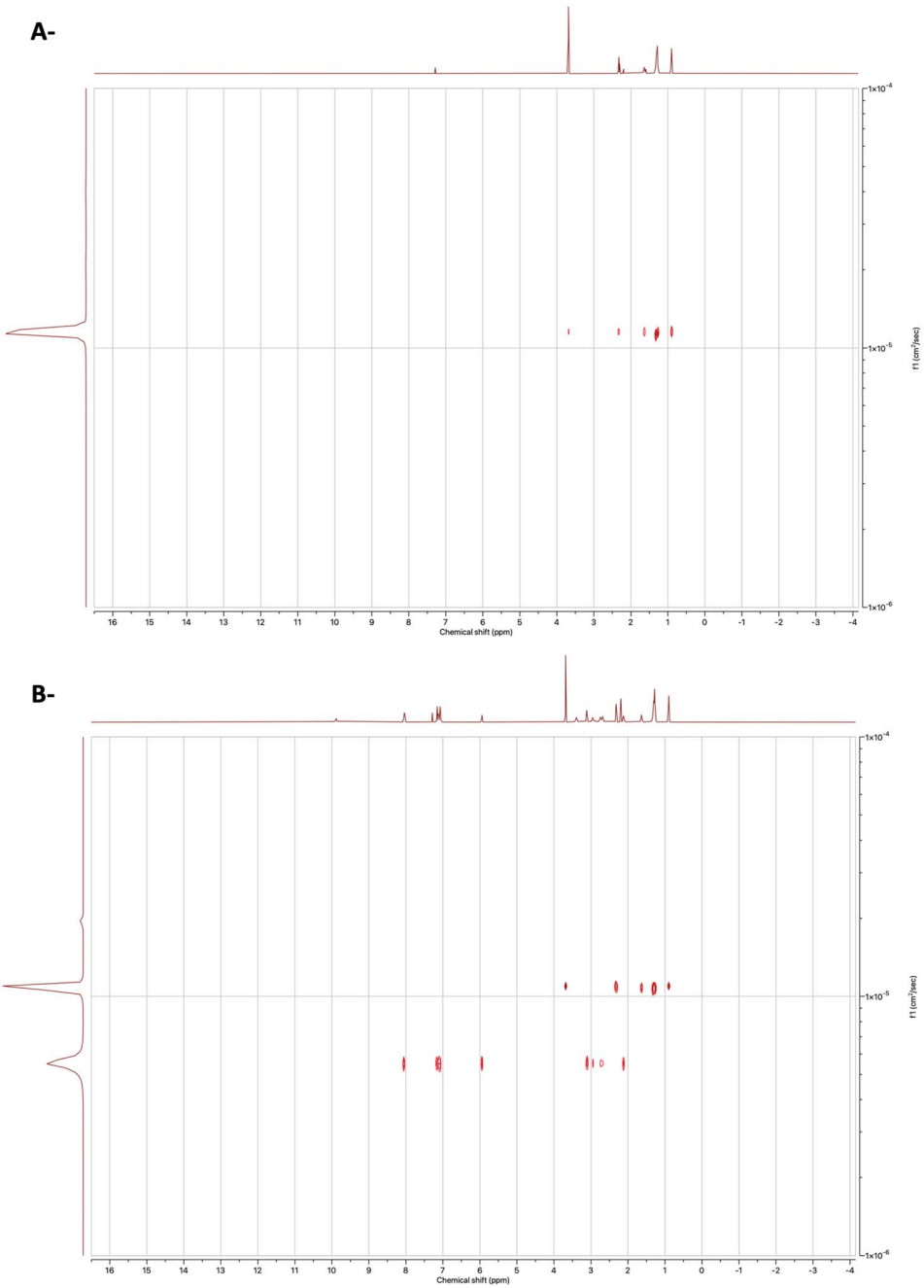

Fig. 3 DOSY ^{1}H spectra of (A) MC and (B) binary 1 : 1 mixture of Drp and MC. The solvent was $CDCl_3$.

The advanced data analysis module of Mestrenova was used to create two-dimensional spectra with NMR chemical shifts (*X*-axis) and the diffusion coefficients (*Y*-axis) and to calculate the diffusion coefficients (*F*). As shown in Fig. 2C and D, the binary mixture exhibited a related diffusion rate compared to the separate compounds (Fig. 2).

Previously, diffusion experiments were performed to study the strength of hydrogen bonding, where the reduction of the diffusion coefficient was directly correlated with the H-bond strength.[47] Herein, following the same methodology, the change in diffusion coefficient was employed to study the strength of interactions present in our system. The change in diffusion coefficients of the binary mixture of Drp and CA was evaluated relative to the individual components in the same solvent (Table 2). A decrease in the diffusion coefficient of CA revealed the strong interactions within the eutectic mixture of the Drp and CA. Generally, diffusion NMR experiments were previously used to study the strength of intermolecular interactions.[48,49] However, to the best of our knowledge, this is the first study that demonstrates the effectiveness of the diffusion NMR technique for evaluating the strength of intermolecular interactions in THEDESs.

To further validate the attained results, a diffusion experiment for the equimolar mixture of Drp and MC was also conducted (Fig. 3). The diffusion coefficients were calculated for the mixture of MC and Drp (Table 2). No significant difference was observed between the diffusion coefficients of the mixture and the individual components, proposing the absence of any interactions. Altogether, the diffusion experiment results of the MC and Drp mixture signify the presence of strong interactions in the eutectic mixture of Drp and CA, as demonstrated previously.

2.1.2 Eutectic mixtures of CA and Arp. Arp belongs to the third-generation antipsychotic agent with unique mechanisms of action and lower incidence rates of motor and metabolic side effects associated with other antipsychotic counterparts.[50] It was approved for the treatment of schizophrenia in 2002.[50] In this work, Arp was selected as the second example to study the mechanism of interactions of the formed eutectic mixtures with CA. The formed eutectic mixture with CA has not been described previously. Structurally, Arp shares the cyclic tertiary amine moiety (Table 1).

Table 3 The prepared binary mixtures of Drp and Arp with CA

Eutectic binary mixtures	Ratios (mol)	Eutectic binary mixture form
CA : Drp	1 : 0 (CA)	—
	0.9 : 0.1 (D1)	Liquid
	0.8 : 0.2 (D2)	Liquid
	0.7 : 0.3 (D3)	Liquid
	0.6 : 0.4 (D4)	Paste
	0.5 : 0.5 (D5)	Paste
	0.4 : 0.6 (D6)	Paste
	0.3 : 0.7 (D7)	Paste
	0.2 : 0.8 (D8)	Paste
	0 : 1 (Drp)	—
CA : Arp	1 : 0 (CA)	—
	0.9 : 0.1 (A1)	Liquid
	0.8 : 0.2 (A2)	Liquid
	0.7 : 0.3 (A3)	Paste
	0.6 : 0.4 (A4)	Paste
	0.5 : 0.5 (A5)	Paste
	0.3 : 0.7 (A7)	Paste
	0.2 : 0.8 (A8)	Paste
	0 : 1 (Arp)	—

Binary mixtures of Arp and CA were prepared with an increasing molar ratio of Arp to CA. Amongst the prepared mixtures, A1 (0.9 : 0.1) and A2 (0.8 : 0.2) were transformed into liquid form, whereas the rest of the binary mixtures were transformed into a pasty form (Table 3).

Interestingly, a ^{1}H NMR study of the binary mixtures in $CDCl_3$ revealed the interaction of the amide group with CA, mainly through hydrogen bonding. This was confirmed by the observed significant downfield chemical shift of the amide proton's peak at 8.18 ppm (1).

Similar to the Drp, the role of the piperazine ring in forming eutectic solvents with CA was evaluated. Interactions of the amine groups in the piperazine ring were predicted *via* the chemical shifts of the adjacent CH_2 protons at 3.20 ppm (2,3). A significant downfield shift of these two $-CH_2$ groups (2,3) was evident with increased concentration of CA in the mixture. As the piperazine ring possesses 2 amines, the lack of downfield shift of the ($-CH_2$) protons at 2.91 ppm (4) confirms that the amine next to the aromatic ring of the piperazine is mainly involved in the CA interactions (Fig. 4A). The positive chemical shift deviation ($\Delta\delta$), as calculated from the protons at 8.18 ppm (1) and 3.20 ppm (2,3) of the Arp with CA, were found to be 0.62 ppm and 0.1 ppm, respectively. The observed downfield shifts imply that these protons are deshielded due to the interactions with the carboxylic acid group of the CA.

Next, validation of the intermolecular interactions using MC, which is not capable of forming acid–base interactions with Arp, was explored. However, MC might be able to form hydrogen bonding with an amide peak at 8.18 ppm. The downfield chemical shifts observed in the Arp and CA eutectic mixture for protons (1–3) were not observed in the case of binary mixtures of MC and Arp (Fig. 4B). This observation demonstrates the essential role of the carboxylic acid protons in mediating the interactions with Arp.

A diffusion experiment confirmed the intermolecular interactions of Arp with CA, as the diffusion spectra of the equimolar eutectic mixture exhibited related diffusion behaviour (Fig. S2 A and B†). On the other hand, the binary mixture of Arp with MC (1 : 1) was similar to the individual components, confirming unrelated diffusion (Fig. S2C†).

2.2 Thermal analysis of the eutectic mixtures

2.2.1 DSC analysis of CA and APIs. Initially, thermal analysis was performed for the drugs and CA separately. Fig. 5A shows the first heating cycle of the DSC thermograms of Arp, Drp, and CA. The melting point (T_m) of CA was observed at 30.4 °C (162.10 J g^{-1}), and the T_m of Arp was seen at 138.8 °C (85.86 J g^{-1}). Another notable observation in the thermogram of Arp was an endothermic event seen at ≈70 °C, which likely

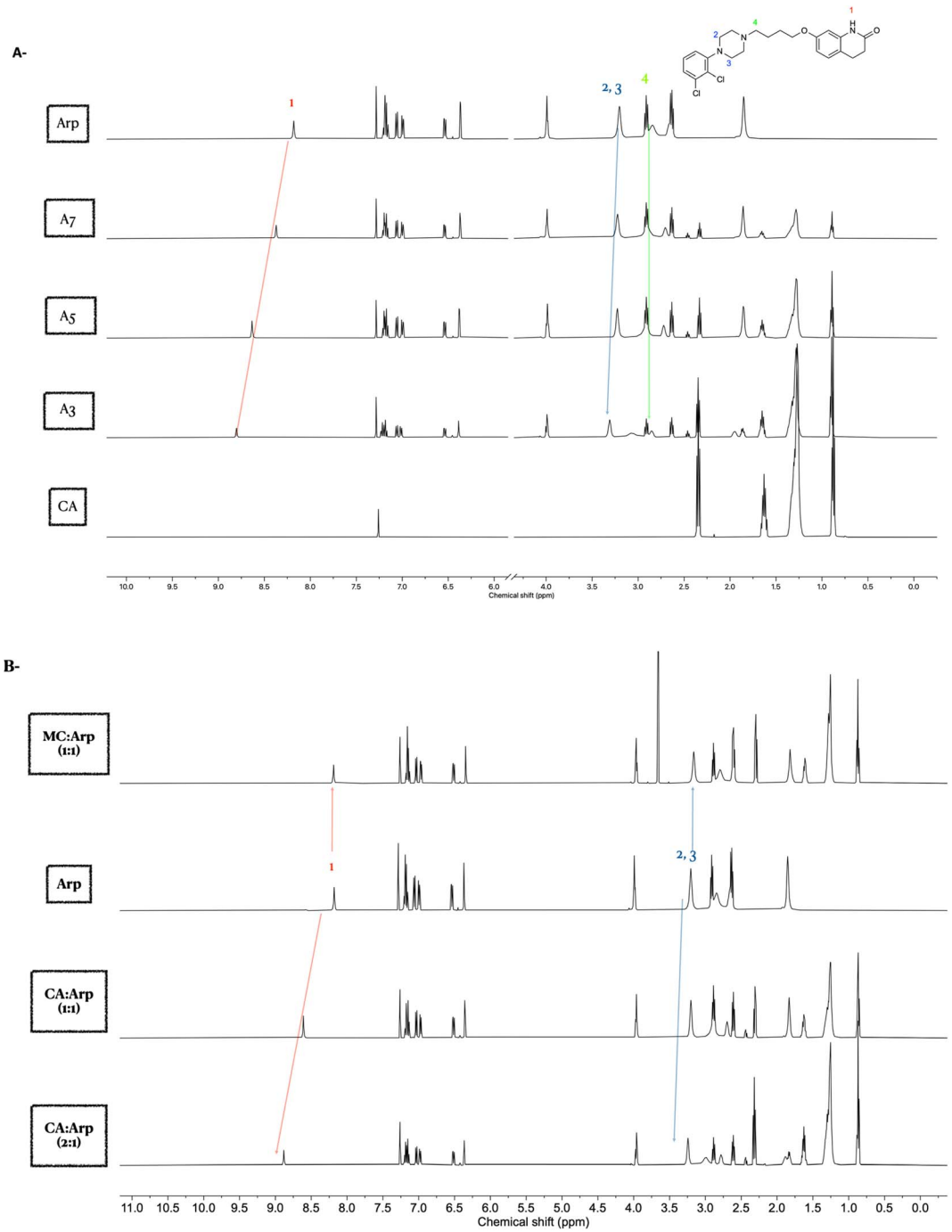

Fig. 4 NMR spectra of Arp–CA eutectic mixture in $CDCl_3$. (A) ^1H NMR of Arp and CA binary mixtures at decreasing molar ratio of CA sowing downfield shifting of peaks at 8.18 and 3.2 ppm. (B) NMR spectra of Arp–CA and Arp–MC equimolar mixtures in $CDCl_3$ solvent.

represents the desolvation of Arp from H_1.[51] The T_m of Drp was observed at 142.62 °C (115.60 J g^{-1}).

Fig. 5B shows the DSC thermograms of the cooling cycle of the raw materials. CA was observed to recrystallise completely at 24 °C (162.12 J g^{-1}). Arp and Drp were all observed to vitrify in the cooling cycle, with glass transitions (Tg) being visible at 25.2 °C (Arp) and 23.7 °C (Drp) (Fig. 5D).

In the second heating cycle (Fig. 5C), the melting endotherm of CA was seen at 30.61 °C. Drp and Arp were observed to recrystallise. Drp exhibited a recrystallisation exotherm at 117 °C, and the T_m of Drp was observed again at 148 °C (90.78 J g^{-1}). Arp was observed to recrystallise at 85.3 °C, with the T_m of Arp visible at 138 °C (84.77 J g^{-1}).

Notably, neither of the drugs recrystallised but rather exhibited vitrification during the cooling cycle. The heating/cooling rate employed during the DSC analysis was 10 °C min^{-1}; this indicates that the drugs belong to Glass Forming Ability (GFA) Class II drugs. Drugs belonging to GFA Class I and

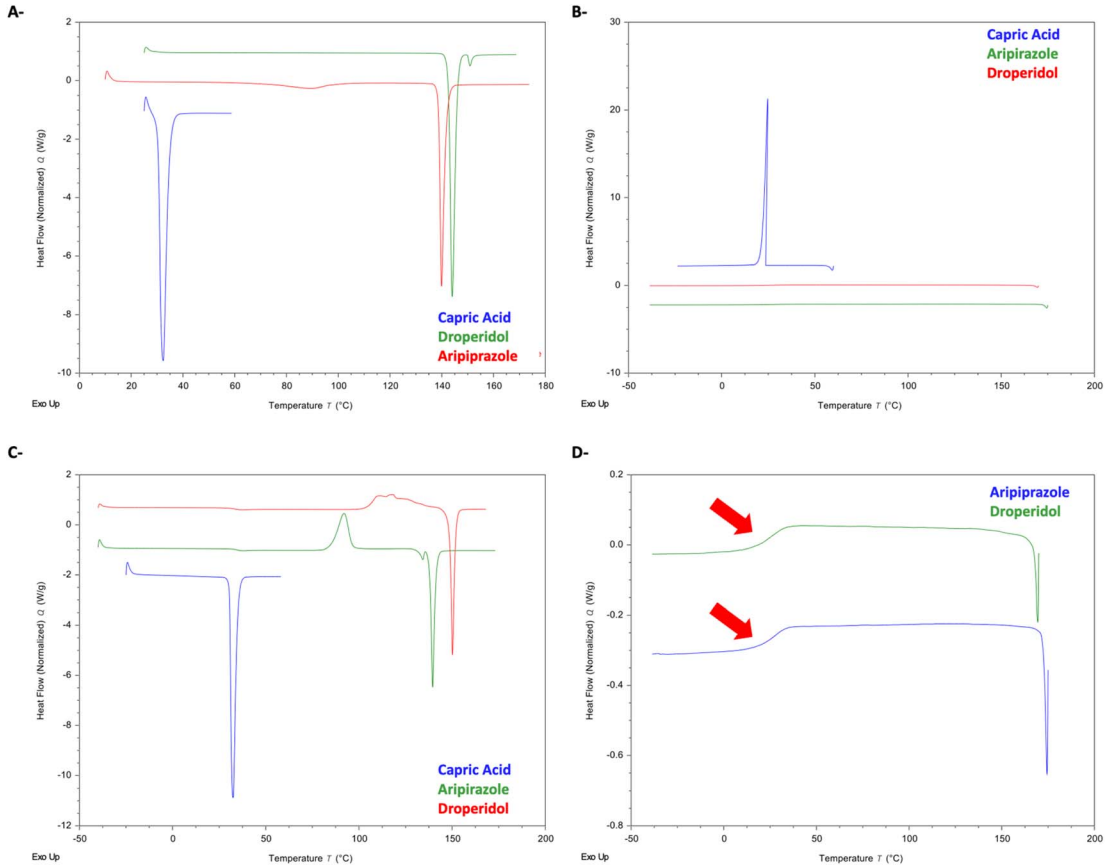

Fig. 5 DSC of raw materials. (A) 1st heating cycle. (B) Cooling cycle. (C) 2nd heating cycle. (D) Observed glass transitions of Drp and Arp and Gef.

II are notable for having weaker crystals with a higher tendency to vitrify and a general tendency to yield comparatively more stable amorphous phases than GFA Class III drugs.[52]

2.2.2 Eutectic mixtures of CA and Drp. Fig. 6 shows the DSC thermograms of the three heating cycles of samples D1, D2, D4, D5, D6, and D8. In Fig. 6A (first heating cycle), the thermograms of samples D1 and D2 (which were observed to form homogenous liquids at room temperature) did not show any endothermic event that corresponded to the melting of Drp or CA, suggesting that at both ratios, a true eutectic liquid is formed with no detectable traces of either CA or Drp precipitates. However, in the cooling cycle of both samples (Fig. 6B), exothermic events were seen at 10.8 °C (D1), and −8.1 °C (D2), with recrystallisation enthalpies of 23.38 J g^{-1} and 20.39 J g^{-1}, respectively. This exothermic event likely corresponds to the recrystallisation of CA, which is corroborated by the endothermic events seen in the second heating cycle, occurring at 14.4 °C (42.24 J g^{-1}) for D2, and 17.70 °C (33.78 J g^{-1}) for D3, which is most likely the depressed melting of CA. This is indicative that the Drp–CA interaction is most likely a weak interaction as the system exhibited phase separation when cooled, with the CA recrystallising out. Precipitated Drp could not be detected in samples D1 and D2, which is to be expected as the high glass-forming tendency of Drp suggests that any phase-separated Drp in the cooling cycle would be present in the amorphous phase.

In the cooling cycle of samples D4, D5, D6, and D8 (all of which were observed to be heterogenous at room temperature), the recrystallisation of CA was not seen. However, baseline changes that likely correspond to the T_g of Drp were seen in all samples. In contrast to samples D1 and D2, the second heating cycle thermograms for samples D4, D5, D6, and D8 showed the recrystallisation and melting peaks in addition to the T_g of Drp. The recrystallisation peak was seen at 96.7 °C (D4), 102.9 °C (D5), 98.8 °C (D6), and 96.7 °C (D8). The melting endotherms were seen at 117.4 °C (23.40 J g^{-1}) for sample D5, 127.2 °C (34.91 J g^{-1}) for sample D5, 124.7 °C (25.37 J g^{-1}) for sample D6, and 129.0 °C (58.71 J g^{-1}) for sample D8, which most likely corresponds to the depressed melting of Drp. Events corresponding to CA were not observed in the samples, most likely due to the loadings being below the limits of detection of DSC.

Fig. 7 shows the DSC thermograms of the Arp–CA eutectic mixtures A3, A5, and A7. In the first heating cycle (Fig. 7A), the desolvation endotherm of form H_1 of Arp was visible in all three thermograms at 58.6 °C, 69.8 °C, and 74.9 °C for samples A3, A5, and A7, respectively. Furthermore, an endothermic event was visible in the thermogram of sample A3 at 18.7 °C (21.96 J g^{-1}), which likely represents the T_m of CA. From the enthalpy values obtained from this endotherm and the T_m of the pure CA sample, we estimate the excess precipitated CA to be approximately 13.5% of the CA content of sample A3. In the cooling cycle (Fig. 7B), no events were observed in the thermogram of

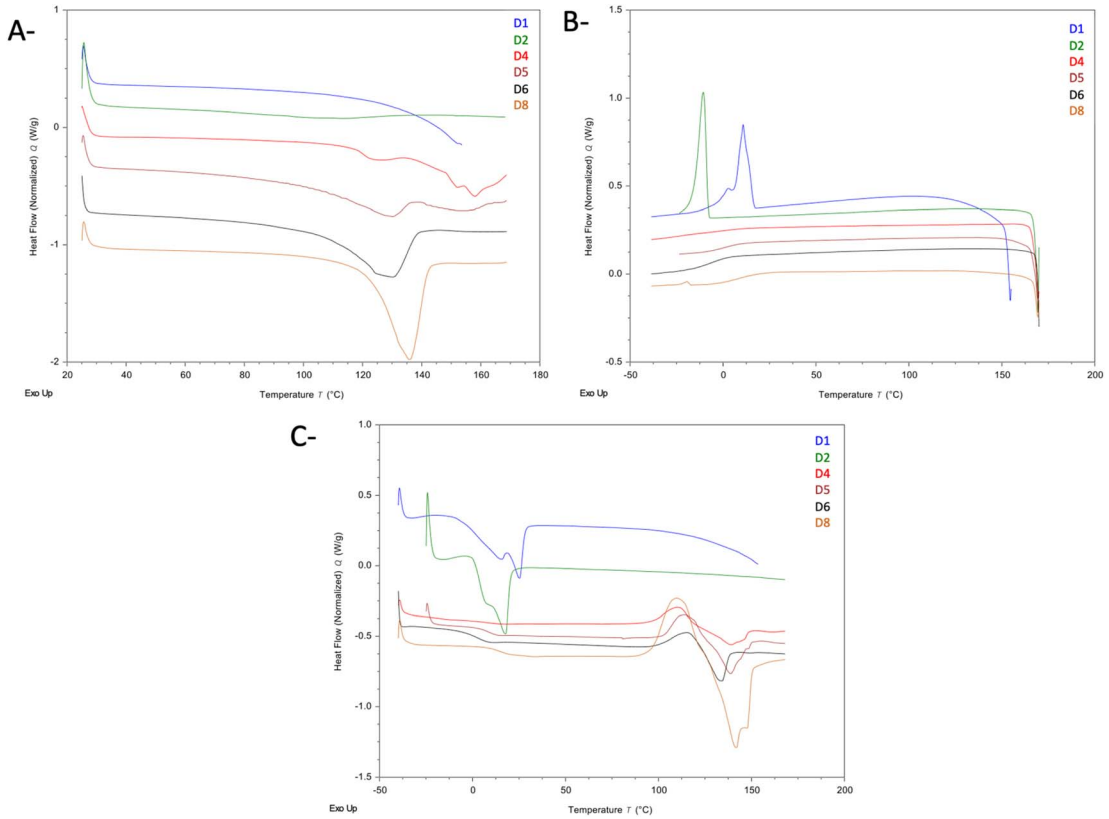

Fig. 6 DSC of Drp–CA eutectic mixtures. (A) 1st heating cycle. (B) Cooling cycle. (C) 2nd heating cycle.

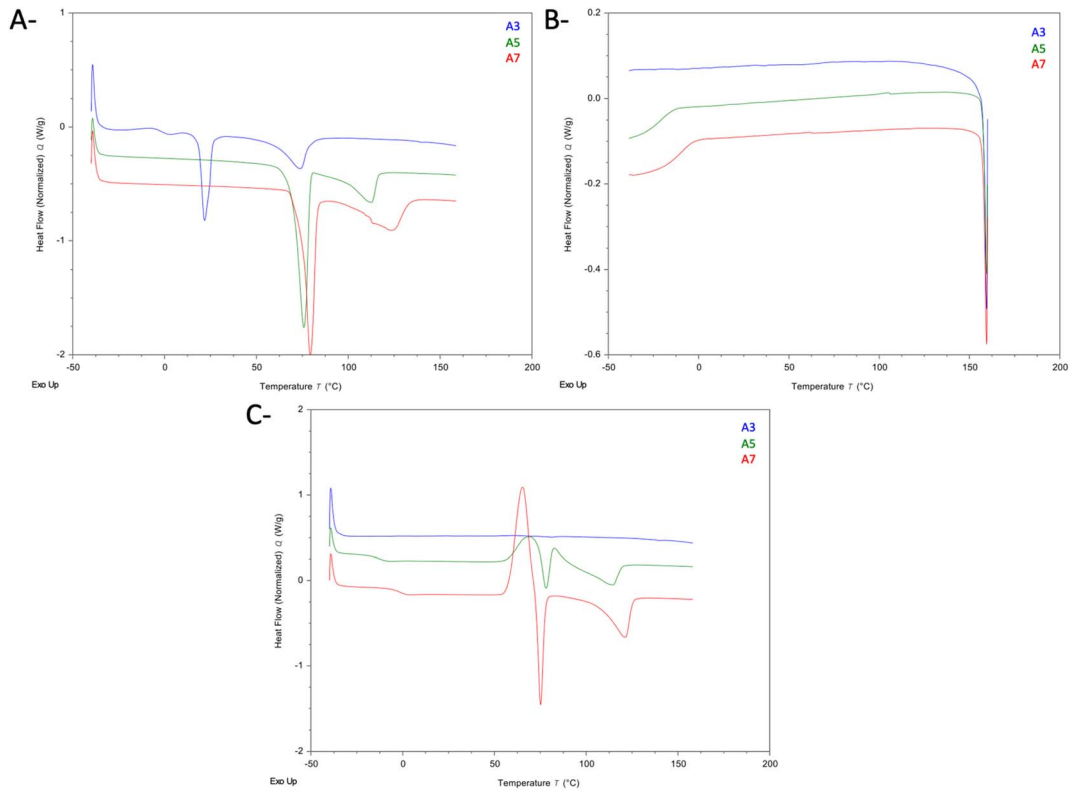

Fig. 7 DSC of Arp–CA eutectic mixtures. (A) 1st heating cycle. (B) Cooling cycle. (C) 2nd heating cycle.

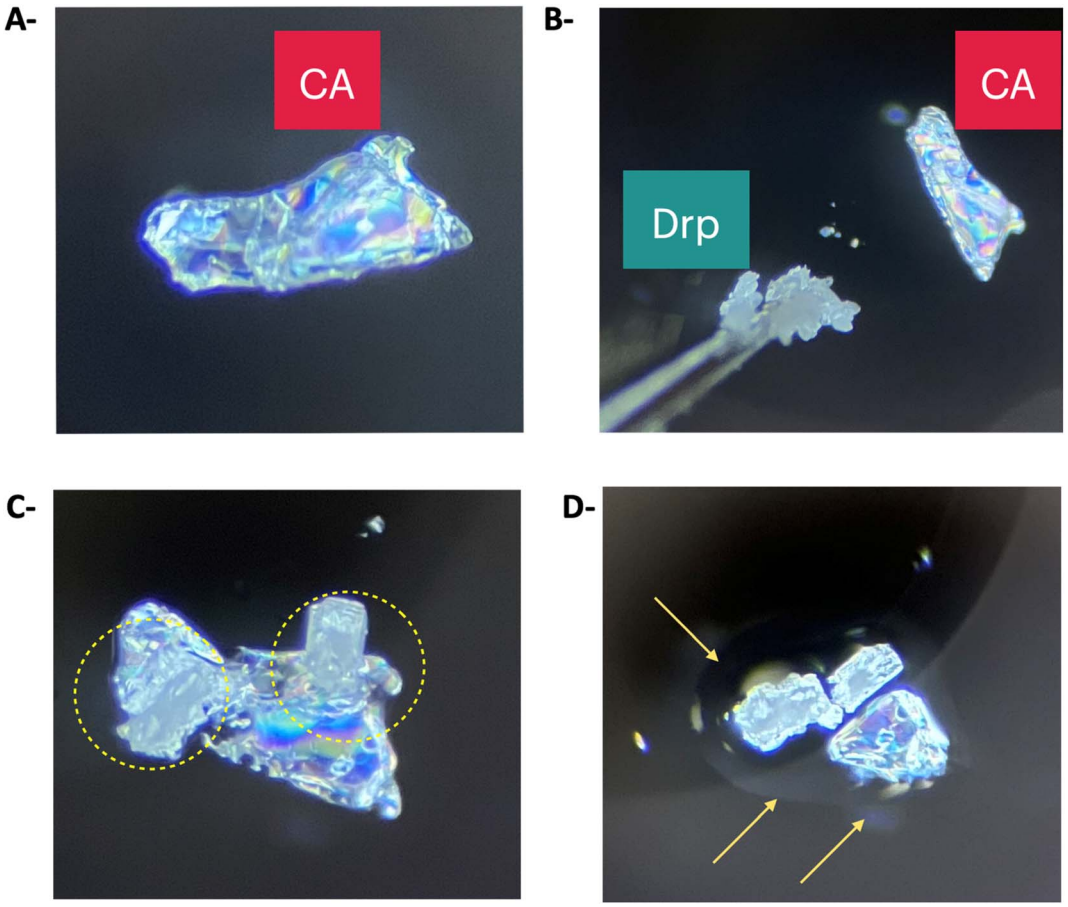

Fig. 8 Images of polarised light microscopy experiment. The experiment was conducted at ambient temperature. (A) Crystal morphology of pure CA. (B) Drp and CAP were brought into physical contact. (C) A liquid intermediate is formed after bringing Drp and CA into contact. A yellow circle highlights the formation of a liquid intermediate. (D) After nearly 30 minutes, a clear liquid phase was formed, highlighted by the arrows.

sample A3. Meanwhile, the T_g of Arp was clearly visible in the thermograms of samples A5 and A7. In the second heating cycle, no events were observable in the thermogram of sample A3. In the thermograms of samples A5 and A7, the T_g of Arp was again visible. Furthermore, the peritectic melting of form H_1 of Arp is again visible in the thermograms of A5 and A7, followed by the phase transformation into the metastable form III polymorph, whose melting is seen at 139 °C.[51,53,54]

In order to validate the hypothesis formulated by the results obtained from both DSC and NMR, a control sample using MC instead of CA was also studied. Drp was used as the model drug for this sample as Drp exhibited the widest concentration range along which a eutectic liquid could be obtained. Fig. S3† shows the DSC results of methyl caprate/Drp sample, along with the thermogram of pure. The T_m of pure methyl caprate was seen at −13 °C (90.25 J g^{-1}). In the thermogram of the mixture (1st heating cycle), both the melting endotherm of methyl caprate and that of Drp were clearly visible at −13 °C (65.84 J g^{-1}) and 140 °C (165.50 J g^{-1}), respectively. In the 2nd heating cycle, the T_m of MC was not visible. However, both the recrystallisation exotherm and T_m of Drp were visible at 46.42 °C and 138.9 °C. The enthalpy of melting of Drp in the second cycle was 100.65 J g^{-1}, corresponding to 61% of the initial amount observed in the first heating cycle, which agrees with the behaviour of pure Drp observed in the thermogram of the pure sample (Fig. 5). The remainder of Drp that was not seen in the thermogram of the second heating cycle is likely converted to the amorphous form of the drug as was seen in the pure sample. The results suggest that there is no interaction between MC and Drp, as the drug melted and recrystallised as independently as a pure sample of the drug was observed to behave, despite the presence of MC in the sample. These findings complement the earlier observations during NMR analyses of the MC–Drp mixture, validating the role of carboxylic acid groups in bringing about interactions necessary to form the DES.

As mentioned earlier, a notable observation was that both Drp and Arp are both GFA Class II drugs,[52] as evidence by their failure to recrystallise on cooling at the cooling rate of 10 °C min^{-1} used throughout the DSC experiments. Similar observations have been previously reported,[18,25,55] indicating some correlation between the ability of a drug to form a THEDES and its GFA class. More specifically, since the GFA class is a proxy for crystal strength,[52] there seems to be a correlation between the crystal strength of a drug and its ability to form THEDES. The control experiment conducted using MC and Drp suggests that the THEDES formation may be brought about by the hydrogen

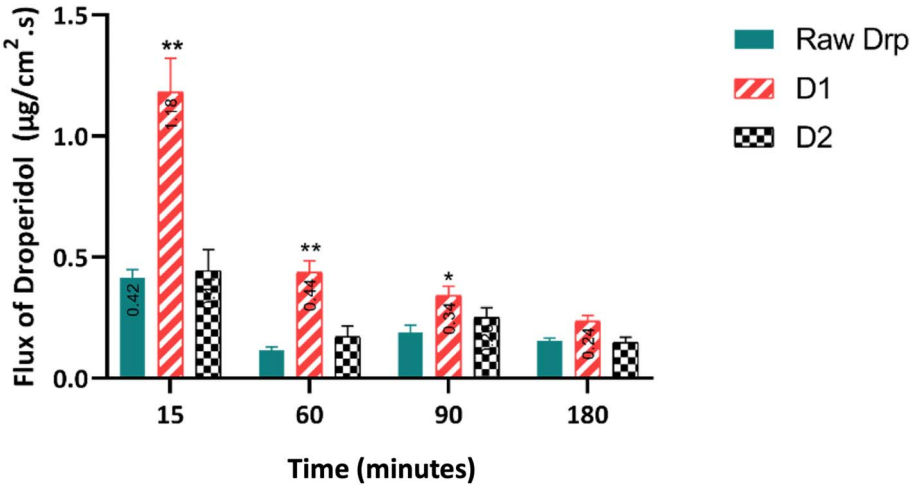

Fig. 9 Flux of Drp (µg cm^{-2} s^{-1}) in everted rats intestinal sac for 180 min. Statistical difference *$p < 0.05$; **$p < 0.01$, two-way ANOVA, compared to raw Drp. Each plot represents the mean ± SEM ($n = 5$).

bonding, as the substitution of the hydrogen bonding forming carboxyl group in CA with the methyl group in MC prevented the formation of a DES. The aforementioned data suggests that the underlying mechanism of DES formation is brought about by the co-former (CA) forming hydrogen bonds with the drug, and due to the weak crystals of the drug (as evidenced by its GFA), the co-former is able to significantly depress its melting,[7] resulting in the formation n of a DES.

2.3 Polarised light microscopy of Drp and CA

Having established comprehensive structural insights explaining the mechanism of interactions and thermal behaviour within the formed eutectic mixtures between Drp and Arp with CA. Next, we studied the time required to attain deep eutectic solvent upon physical contact between CA and Drp at ambient temperature. When a crystal of Drp was brought into contact with a crystal of CA at ambient temperature (Fig. 8A and B), they began interacting immediately, and the formation of a liquid phase was observed, marked by the circles in Fig. 8C. The morphology of the formed mixture of CA and Drp after 30 minutes differed significantly from the crystal shapes of pure CA and Drp (Fig. 8D). The rapid phase transition from the solid to the liquid state when Drp is brought into contact with CA shows that the formation of the DES is a rapid and spontaneous process. Furthermore, since the crystals formed a DES under ambient conditions without the need for heating and/or agitation, it shows that the reported system is a good candidate to be scaled up for commercial applications in the pharmaceutical industry, therefore achieving higher drug solubilization while maintaining green processing, without the need to incorporate organic solvents.

2.4 Everted rat intestinal sac (ERIS)

With the developed THEDESs in our hands, we sought to study the advantages of adopting THEDESs to enhance the permeability and adoption of Drp using ERIS.

ERIS is a technique widely employed in pharmaceutical research to study the systemic availability, absorption, permeation, and interactions of drugs. By using this tool, the permeation and absorption of drugs across the intestinal epithelium of rats are studied by measuring their flux.[56] DESs generally have better absorption and permeation due to their ability to improve the poor water solubility and low dissolution rate of APIs.[57,58]

Forming hydrophobic THEDESs with CA would increase the hydrophobic features of the drugs. Nevertheless, the mixture would exhibit improved permeability and absorption. This was clearly demonstrated in the present study (Fig. 9). All the tested samples exhibited time-dependent intestinal flux that gradually decreased over time. Notably, D1 achieved the highest flux of 1.182 mg cm^{-2} s^{-1} at 15 minutes, remarkably exceeding the other formulations. While Drp and D2 showed similar profiles, D1 consistently maintained the highest flux throughout the 3 h. This superior permeation profile observed with D1 was statistically confirmed (p-value >0.05). The results demonstrated superior drug absorption when using and maintaining green processing conditions without incorporating organic solvents.

3 Conclusions

In this work, novel DESs comprising CA with two drugs, Drp and Arp, bearing a cyclic tertiary amine moiety, have been investigated. The mechanism of interactions responsible for forming these eutectic mixtures was studied in detail using liquid-state NMR analyses, DSC analysis and polarised light microscopy. 1D NMR results demonstrate the role of tertiary amine in forming eutectic mixtures with CA. In addition, we demonstrated the utility of diffusion NMR experiments in studying the intermolecular interactions in eutectic mixtures. This is the first demonstration of the use of diffusion NMR to study eutectic mixtures of APIs in solution. Thermal analysis of the two drugs revealed that they have a low tendency to recrystallise upon melting but rather vitrify into amorphous solid, which appears to play a major role in DES formation when mixed with CA.

Studying the flux of Drp using an everted rat intestinal sac technique has demonstrated the superior permeability and absorption of D1 formulation compared to Drp. Collectively, this work laid the foundation for developing novel eutectic mixtures of APIs with capric acid accompanied by a demonstration of enhanced absorption and permeability.

4 Experimental

4.1 Materials and general remarks

Capric acid (CA) and methyl caprate (MC) were purchased from Sigma-Aldrich. Droperidol (Drp) and Aripiprazole (Arp) were kindly provided as gifts from Jordanian Pharmaceutical Manufacturing Company (JPM), Amman, Jordan. All chemicals were used as such without further purification. Full characterisation of the drugs was performed using NMR techniques to demonstrate their purity. Deuterated solvents for NMR were purchased from Cambridge Isotope Laboratories and Sigma-Aldrich.

4.2 Preparation of eutectic physical mixtures

Mixtures of Drp–CA and Arp–CA were prepared in approximately 50 mg aliquots at appropriate molar ratios. The mixtures were held shaking in a water bath 40 °C for 24 h until homogenous or/and clear liquid was attained. The details of the prepared binary mixture are shown in Table 3.

4.3 NMR experiment

Nuclear magnetic resonance spectra were recorded in deuterated solvents $CDCl_3$ using Bruker Advance III (500 MHz) spectrometers operating at 25 °C with a BBFO+ probe. Drp, Arp, or THEDESs (with equivalent amounts of APIs) samples were prepared by direct dissolving in the deuterated solvent and dissolved completely before submitting. The diffusion data were acquired using the ledbpgp2s pulse sequence, with d_1 = 4 s, ns typically 4, 10 diffusion power levels ranging from 2% to 98%, D20 of 0.05 s and D21 of 0.005 s. P30 was 1 ms. The advanced data analysis module of Mestrenova was used to create two-dimensional spectra with NMR chemical shifts (*X*-axis) and the diffusion coefficients (*Y*-axis) and to calculate the diffusion coefficients (*F*).

4.4 NMR characterisation of the individual compounds

4.4.1 Droperidol. ^{1}H NMR (500 MHz, DMSO) δ 10.91 (s, 1H), 8.24–7.94 (m, 2H), 7.59–7.17 (m, 2H), 7.15–6.72 (m, 4H), 5.82 (td, J = 3.5, 1.7 Hz, 1H), 3.26–2.88 (m, 4H), 2.65 (t, J = 5.6 Hz, 2H), 2.45–2.28 (m, 2H), 1.88 (t, J = 6.9 Hz, 2H).

^{13}C NMR (126 MHz, DMSO-d_6) δ 198.98, 166.31, 164.31, 153.37, 134.25, 134.23, 131.36, 131.28, 130.75, 130.33, 128.91, 123.56, 121.68, 121.06, 116.16, 115.99, 109.37, 108.76, 56.89, 51.74, 49.67, 36.16, 27.35, 22.11.

4.4.2 Aripiprazole. ^{1}H NMR (500 MHz, $CDCl_3$) δ 8.18 (s, 1H), 7.23–7.12 (m, 2H), 7.06 (d, J = 8.3 Hz, 1H), 6.99 (dd, J = 7.5, 2.1 Hz, 1H), 6.54 (dd, J = 8.3, 2.4 Hz, 1H), 6.37 (d, J = 2.4 Hz, 1H), 4.21–3.79 (m, 2H), 3.20 (s, 4H), 3.05–2.76 (m, 6H), 2.63 (dq, J = 11.6, 6.3 Hz, 5H), 2.01–1.56 (m, 5H).

^{13}C NMR (126 MHz, $CDCl_3$) δ 171.62, 158.50, 138.17, 134.10, 128.71, 127.60, 127.54, 125.09, 118.82, 115.88, 108.64, 102.20, 67.64, 57.92, 53.00, 31.10, 27.03, 24.60, 22.63.

4.4.3 Capric acid. ^{1}H NMR (500 MHz, DMSO-d_6) δ 11.97 (s, 1H), 2.18 (t, J = 7.4 Hz, 2H), 1.48 (p, J = 6.9 Hz, 2H), 1.25 (d, J = 3.1 Hz, 12H), 0.86 (t, J = 6.8 Hz, 3H).

^{13}C NMR (126 MHz, DMSO) δ 174.96, 34.12, 31.74, 29.34, 29.22, 29.12, 29.01, 24.96, 22.56, 14.40.

4.4.4 Methyl caprate. ^{1}H NMR (500 MHz, $CDCl_3$) δ 3.69 (s, 3H), 2.32 (t, J = 7.6 Hz, 2H), 1.64 (p, J = 7.2 Hz, 2H), 1.45–1.16 (m, 12H), 0.90 (t, J = 6.8 Hz, 3H).

4.4.5 DSC. Differential scanning calorimetry (DSC) analyses were conducted using a TA instrument discovery series DSC25 (TA Instruments, Newcastle, USA). Scans were acquired using a heat–cool–reheat cycle. Samples containing droperidol and aripiprazole (both pure drug and formulations) were equilibrated at room temperature for 1 minute, then ramped to 170 °C, followed by cooling to −20 °C, then reheating to 170 °C. Nitrogen purge gas was used for all runs, with a constant flow rate of 50 mL min^{-1}. All samples were analysed using a heating rate or cooing rate of 10 °C min^{-1}. Standard aluminium pans containing samples weighing 2–4 mg were used for all scans. A known amount (2–4 mg) of the tested samples, including pure drugs and THEDESs, was used as such.

4.5 Polarised light microscope

The polarised light microscopy experiment was performed using an MEIJI TECHNO (EMZ-13TR) polarising optical microscope.

4.5.1 Everted rat intestinal sac (ERIS). Three solutions of Drp, D1 and D2 were prepared by dissolving an amount equivalent to 30 mg droperidol in 250 mL Krebs buffer (pH 7.2), achieving a final concentration of 0.12 mg mL^{-1}. The ERIS technique was carried out as previously described.[59] The sacs, each measuring 3 cm in length, were obtained from the gastrointestinal tract of four mature male Sprague Dawley rats. These were then divided at random into three groups, each containing five sacs. Then, they were incubated in Krebs buffer for 15 minutes at room temperature. The sacs were incubated in a shaking water bath (50 RPM) at 37 °C. At specific time intervals (15, 60, 90, and 180 minutes), sacs were removed, and the samples were collected using syringes, which were refrigerated until HPLC analysis.

4.6 Statistical analysis

To determine the significance between groups, a two-way ANOVA test using GraphPad Prism version 7.01. Values are expressed as mean ± standard error of the mean (SEM). Results were considered significant for p-values ≤0.05.

4.7 HPLC analysis

The analysis of Drp using HPLC was conducted as described by Yeniceli *et al.* (2007).[60] Briefly, the detection wavelengths were set at 283 nm. A 4.6 mm × 25 cm separation column packed with 5 μm L1 beads (Supelco, USA) was used as the stationary phase. The mobile phase consisted of methanol–water (30 : 70,

v/v) at pH 3.5. The flow rate was set to 0.8 mL min^{-1}, and the injection volume was 5 μL. A calibration curve of Drp was constructed and found to be linear with an R2 of 0.998 over the tested range of concentrations (Fig. S4†). Spiking with Krebs buffer was carried out over the same range of concentrations as the calibration curve to ensure the compatibility of the method for the ERIS experiment.

Conflicts of interest

There are no conflicts to declare.

Acknowledgements

The authors would like to thank the Deanship of Scientific Research at the University of Petra for the financial support of this study. In addition, the author would like to thank Ghayda Al Dabet for her help conducting the Everted rat intestinal sac (ERIS).

References

1 D. Carriazo, M. C. Serrano, M. C. Gutiérrez, M. L. Ferrer and F. del Monte, *Chem. Soc. Rev.*, 2012, **41**, 4996–5014.
2 M. Deetlefs and K. R. Seddon, *Green Chem.*, 2010, **12**, 17–30.
3 F. Al-Akayleh, M. Ali, M. Ghareeb and M. Al-Remawi, *Drug Delivery Sci. Technol.*, 2019, **53**, 101159.
4 V. Renza-Diaz, M. Gonzalez-Hernández, K. D. Pantoja and R. F. D'Vries, *CrystEngComm*, 2021, **23**, 4985–4993.
5 A. P. Abbott, G. Capper, D. L. Davies, R. K. Rasheed and V. Tambyrajah, *Chem. Commun.*, 2003, 70–71.
6 N. Schaeffer, J. H. Conceição, M. A. Martins, M. C. Neves, G. Pérez-Sánchez and J. R. Gomes, *Green Chem.*, 2020, **22**(9), 2810–2820.
7 A. Paiva, R. Craveiro, I. Aroso, M. Martins, R. L. Reis and A. R. C. Duarte, *ACS Sustain. Chem. Eng.*, 2014, **2**, 1063–1071.
8 S. Miao, R. Atkin and G. Warr, *Green Chem.*, 2022, **24**, 7281–7304.
9 A. R. C. Duarte, A. S. D. Ferreira, S. Barreiros, E. Cabrita, R. L. Reis and A. Paiva, *Eur. J. Pharm. Biopharm.*, 2017, **114**, 296–304.
10 F. Al-Akayleh, M. Al-Remawi, A. Agha and E. Abu-Nameh, *Jordan J. Chem.*, 2023, **18**, 53–76.
11 J. A. Kist, H. Zhao, K. R. Mitchell-Koch and G. A. Baker, *J. Mater. Chem. B*, 2021, **9**, 536–566.
12 D. K Luhaibi, H. H. M. Ali, I. Al-Ani, N. Shalan, F. Al-Akayleh, M. Al-Remawi and M. Khanfar, *Molecules*, 2023, **28**(19), 6927.
13 B. Alkhawaja, F. Al-Akayleh, A. Al-Khateeb, J. Nasereddin, B. Ghanim, A. Bolhuis and N. Qinna, *Molecules*, 2023, **28**, 2402.
14 A. Nakaweh, F. Al-Akayleh, M. Al-Remawi, Q. Abdallah and A. Agha, *J. Pharm. Innovation*, 2024, **19**, 1–11.
15 L. Al-Mawla, F. Al-Akayleh, S. Daadoue, W. Mahyoob, B. Al-Tameemi, M. Al-Remawi and A. Agha, *J. Pharm. Innovation*, 2023, **18**, 2196–2209.
16 B. Olivares, F. Martínez, L. Rivas, C. Calderón, J. M. Munita and P. R. Campodonico, *Sci. Rep.*, 2018, **81**(8), 1–12.
17 D. Arnodo, C. Meazzo, S. Baldino, M. Blangetti and C. Prandi, *Materials*, 2023, **29**(36), e202300820.
18 F. Al-Akayleh, S. Adwan, M. Khanfer, N. Idkaidek and M. Al-Remawi, *AAPS PharmSciTech*, 2021, **22**, 1–11.
19 J. Lee, D. Jung and K. Park, *TrAC, Trends Anal. Chem.*, 2019, **118**, 853–868.
20 L. Al-Mawla, F. Al-Akayleh, S. Daadoue, W. Mahyoob, B. Al-Tameemi, M. Al-Remawi, S. Adwan and A. S. A. Agha, *J. Pharm. Innovation*, 2023, **18**(4), 2196–2209.
21 F. Al-Akayleh, R. M. Khalid, D. Hawash, E. Al-Kaissi, I. S. I. Al-Adham, N. Al-Muhtaseb, N. Jaber, M. Al-Remawi and P. J. Collier, *Lett. Appl. Microbiol.*, 2022, **75**, 607–615.
22 J. M. Silva, C. V. Pereira, F. Mano, E. Silva, V. I. B. Castro, I. Sá-Nogueira, R. L. Reis, A. Paiva, A. A. Matias and A. R. C. Duarte, *ACS Appl. Bio Mater.*, 2019, **2**, 4346–4355.
23 R. V. Rariy, A. Fleming, J. C. Hirsh, S. Saim, R. K. Varanasi, WO2022107182A1, 2020.
24 K. Bialek, Z. Wojnarowska, M. Skotnicki, B. Twamley, M. Paluch and L. Tajber, *Pharmaceutics*, 2021, **13**, 2125.
25 B. Alkhawaja, F. Al-Akayleh, J. Nasereddin, S. A. Malek, N. Alkhawaja, M. Kamran, Z. Al-Rubaye, M. Smairat, M. Al-Remawi and W. S. Aburayyan, *AAPS PharmSciTech*, 2023, **24**, 1–12.
26 M. H. Zainal-Abidin, M. Hayyan and W. F. Wong, *J. Ind. Eng. Chem.*, 2021, **97**, 142–162.
27 S. Kim, J. Chen, T. Cheng, A. Gindulyte, J. He, S. He, Q. Li, B. A. Shoemaker, P. A. Thiessen, B. Yu, L. Zaslavsky, J. Zhang and E. E. Bolton, *Nucleic Acids Res.*, 2021, **49**, D1388–D1395.
28 A. Turek, A. Borecka, H. Janeczek, M. Sobota and J. Kasperczyk, *Int. J. Pharm.*, 2018, **548**, 159–172.
29 *Risperidone: Uses, Interactions, Mechanism of Action*, DrugBank, Online.
30 S. D. Roy and G. L. Flynn, *Pharm. Res.*, 1989, **6**, 147–151.
31 *Fentanyl: Uses, Interactions, Mechanism of Action*, DrugBank, Online.
32 DrugBank, Online, *Levofloxacin: Uses, Interactions, Mechanism of Action*.
33 The National Center for Biotechnology Information (NCBI), *Levofloxacin|C18H20FN3O4|CID 149096 – PubChem*.
34 Droperidol|C22H22FN3O2 – PubChem.
35 *Droperidol: Uses, Interactions, Mechanism of Action*, DrugBank, Online.
36 *Aripiprazole: Uses, Interactions, Mechanism of Action*, DrugBank, Online.
37 Decanoic acid|C10H20O2 – PubChem.
38 Methyl decanoate|C11H22O2 – PubChem.
39 L. K. Foo, S. B. Duffull, L. Calver, J. Schneider and G. K. Isbister, *Br. J. Clin. Pharmacol.*, 2016, **82**, 1550.
40 T. Y. Wu, N. Tien, C. L. Lin, Y. C. Cheah, C. Y. Hsu, F. J. Tsai and Y. P. Lim, *Front. Biomed.*, 2023, **10**, 1137977.
41 D. Cisewski, B. Long and M. Gottlieb, *Am. J. Emerg. Med.*, 2022, **53**, 180–184.
42 H. Saluja, A. Mehanna, R. Panicucci and E. Atef, *Molecules*, 2016, **21**, 719.
43 H. Ali, M. Ghareeb, M. Al-Remawi and F. Al-Akayleh, *Trop. J. Pharm. Res.*, 2020, **19**, 361–369.

44 H. Wang, J. Cui, H. Li, Y. Zhao and J. Wang, *J. Mol. Struct.*, 2019, **1179**, 57–64.
45 J. Ho, C. J. Easton and M. L. Coote, *J. Am. Chem. Soc.*, 2010, **132**, 5515–5521.
46 T. D. A. Senra, A. Khoukh and J. Desbrières, *Carbohydr. Polym.*, 2017, **156**, 182–192.
47 Y. Cohen, L. Avram and L. Frish, *Angew. Chem., Int. Ed.*, 2005, **44**, 520–554.
48 S. R. Chaudhari and N. Suryaprakash, *J. Mol. Struct.*, 2012, **1016**, 163–168.
49 Y. Cohen, L. Avram and L. Frish, *Angew. Chem., Int. Ed.*, 2005, **44**, 520–554.
50 A. Preda and B. B. Shapiro, *Expert Opin. Drug Saf.*, 2020, **19**, 1529–1538.
51 D. E. Braun, T. Gelbrich, V. Kahlenberg, R. Tessadri, J. Wieser and U. J. Griesser, *Cryst. Growth Des.*, 2009, **9**, 1054–1065.
52 P. Panini, M. Rampazzo, A. Singh, F. Vanhoutte and G. Van den Mooter, *Pharmaceutics*, 2019, **11**(10), 529.
53 A. P. Ayala, S. B. Honorato, J. M. Filho, D. Grillo, M. Quintero, F. Gilles and G. Polla, *Vib. Spectrosc.*, 2010, **54**, 169–173.
54 D. E. Braun, T. Gelbrich, V. Kahlenberg, R. Tessadri, J. Wieser and U. J. Griesser, *J. Pharm. Sci.*, 2009, **98**, 2010–2026.
55 S. Daadoue, M. Al-Remawi, L. Al-Mawla, N. Idkaidek, R. M. Khalid and F. Al-Akayleh, *J. Mol. Liq.*, 2022, **345**, 117347.
56 M. A. Alam, F. I. Al-Jenoobi and A. M. Al-Mohizea, *J. Pharm. Pharmacol.*, 2012, **64**, 326–336.
57 S. Trombino, C. Siciliano, D. Procopio, F. Curcio, A. S. Laganà, M. L. Di Gioia and C. Roberta, *Pharmaceutics*, 2022, **14**, 333.
58 S. Chakraborty, R. Y. Sathe, J. H. Chormale, A. Dangi, P. V. Bharatam and A. K. Bansal, *Pharmaceutics*, 2023, **15**(9), 2351.
59 N. A. Qinna, M. H. Shubbar, K. Z. Matalka, N. Al-Jbour, M. A. Ghattas and A. A. Badwan, *J. Pharm. Sci.*, 2015, **104**, 257–265.
60 D. Yeniceli, D. Dogrukol-Ak and M. Tuncel, *Chromatographia*, 2007, **66**, 37–43.